High-mode spoof SPP of periodic metal grooves for ultra-sensitive terahertz sensing

Haizi Yao[1] and Shuncong Zhong[1,2,*]

[1] *Laboratory of Optics, Terahertz and Non-Destructive Testing, School of Mechanical Engineering and Automation, Fuzhou University,No.2 Campus Road, Fuzhou 350108, P. R. China*

[2] *Fujian Key Laboratory of Medical Instrument and Pharmaceutical Technology, No.2 Campus Road, Fuzhou 350108, P.R. China*

[*] *zhongshuncong@hotmail.com*

Abstract: We report terahertz surface plasmon resonance (SPR) sensing based on prism-coupling to the spoof surface plasmon polariton (SSPP) mode existing on periodically grooved metal films. It was demonstrated that, except for the fundamental mode of the SSPP, there was also a higher mode SSPP wave when the depth of groove was larger. Both fundamental and high-order modes of SSPP could be used for terahertz sensing. We compared the performance of different modes of SSPP on the sensing sensitivity using both reflection amplitude and phase-jump information. The results indicated that the gap distance between the prism base and the metal film had a significant influence on the reflectivity of SPR sensing by affecting the coupling efficiency of an evanescent wave to an SSPP wave; also, high-order mode SSPP-based sensing had a high sensitivity of up to 2.27 THz/RIU, which nearly doubled the sensitivity of the fundamental mode. The application of high-mode SSPP has enormous potential for ultra-sensitive SPR sensing in the terahertz regime.

OCIS codes: (300.6495) Spectroscopy, terahertz; (280.1415) Biological sensing and sensors.

References and links

1. D. Hornauer, H. Kapitza, and H. Raether, "The dispersion relation of surface plasmons on rough surfaces," J. Phys. D: Appl. Phys. **7**(9), L100 (1974).
2. H. Raether, *Surface plasmons on smooth surfaces* (Springer, 1988).
3. S. A. Maier, *Plasmonics: Fundamentals and Applications: Fundamentals and Applications* (Springer, 2007).
4. R. Wood, "XLII. On a remarkable case of uneven distribution of light in a diffraction grating spectrum," The London, Edinburgh, and Dublin Philosophical Magazine and Journal of Science **4**(21), 396-402 (1902).
5. E. Kretschmann, and H. Raether, "Radiative decay of non radiative surface plasmons excited by light(Surface plasma waves excitation by light and decay into photons applied to nonradiative modes)," Zeitschrift Fuer Naturforschung, Teil A **23**, 2135 (1968).
6. A. Otto, "Excitation of nonradiative surface plasma waves in silver by the method of frustrated total reflection," Z. Angew. Phys. **216**(4), 398-410 (1968).
7. R. Slavík, and J. Homola, "Ultrahigh resolution long range surface plasmon-based sensor," Sens. Actuators, B **123**(1), 10-12 (2007).
8. K. S. Phillips, and Q. J. Cheng, "Surface Plasmon Resonance," in *Molecular Biomethods Handbook*(Springer, 2008).
9. G. Gauglitz, and G. Proll, "Strategies for label-free optical detection," in *Biosensing for the 21st Century*(Springer, 2008).
10. R. Georgiadis, K. Peterlinz, and A. Peterson, "Quantitative measurements and modeling of kinetics in nucleic acid monolayer films using SPR spectroscopy," J. Am. Chem. Soc. **122**(13), 3166-3173 (2000).
11. J. M. McDonnell, "Surface plasmon resonance: towards an understanding of the mechanisms of biological molecular recognition," Curr. Opin. Chem. Biol. **5**(5), 572-577 (2001).
12. J. F. Federici, B. Schulkin, F. Huang, D. Gary, R. Barat, F. Oliveira, and D. Zimdars, "THz imaging and sensing for security applications—explosives, weapons and drugs," Semicond. Sci. Technol. **20**(7), S266 (2005).
13. R. Piesiewicz, T. Kleine-Ostmann, N. Krumbholz, D. Mittleman, M. Koch, J. Schoebel, and T. Kurner, "Short-range ultra-broadband terahertz communications: Concepts and perspectives," Antennas and Propagation

Magazine, IEEE **49**(6), 24-39 (2007).
14. T. Globus, D. Woolard, T. Khromova, T. Crowe, M. Bykhovskaia, B. Gelmont, J. Hesler, and A. Samuels, "THz-spectroscopy of biological molecules," J. Biol. Phys. **29**(2-3), 89-100 (2003).
15. M. Walther, P. Plochocka, B. Fischer, H. Helm, and P. Uhd Jepsen, "Collective vibrational modes in biological molecules investigated by terahertz time - domain spectroscopy," Biopolymers **67**(4 - 5), 310-313 (2002).
16. H. Barlow, and A. Cullen, "Surface waves," Proceedings of the IEE-Part III: Radio and Communication Engineering **100**(68), 329-341 (1953).
17. J. Pendry, L. Martin-Moreno, and F. Garcia-Vidal, "Mimicking surface plasmons with structured surfaces," Science **305**(5685), 847-848 (2004).
18. F. Garcia-Vidal, L. Martin-Moreno, and J. Pendry, "Surfaces with holes in them: new plasmonic metamaterials," J. Opt. A: Pure Appl. Opt. **7**(2), S97 (2005).
19. C. R. Williams, S. R. Andrews, S. Maier, A. Fernández-Domínguez, L. Martín-Moreno, and F. García-Vidal, "Highly confined guiding of terahertz surface plasmon polaritons on structured metal surfaces," Nat. Photonics **2**(3), 175-179 (2008).
20. A. Rusina, M. Durach, and M. I. Stockman, "Theory of spoof plasmons in real metals," in *SPIE NanoScience+ Engineering*(International Society for Optics and Photonics, 2010), pp. 77572R-77572R-77576.
21. R. F. Aroca, D. J. Ross, and C. Domingo, "Surface-enhanced infrared spectroscopy," Appl. Spectrosc. **58**, 324A-338A (2004).
22. M. Osawa, "Surface-enhanced infrared absorption," in *Near-Field Optics and Surface Plasmon Polaritons*(Springer, 2001).
23. F. Miyamaru, M. Takeda, T. Suzuki, and C. Otani, "Highly sensitive surface plasmon terahertz imaging with planar plasmonic crystals," Opt. Express **15**(22), 14804-14809 (2007).
24. M. Golosovsky, V. Lirtsman, V. Yashunsky, D. Davidov, and B. Aroeti, "Midinfrared surface-plasmon resonance: A novel biophysical tool for studying living cells," J. Appl. Phys. **105**(10), 102036 (2009).
25. B. Ng, J. Wu, S. M. Hanham, A. I. Fernández - Domínguez, N. Klein, Y. F. Liew, M. B. Breese, M. Hong, and S. A. Maier, "Spoof Plasmon Surfaces: A Novel Platform for THz Sensing," Advanced Optical Materials **1**(8), 543-548 (2013).
26. T. Jiang, L. Shen, X. Zhang, and L.-X. Ran, "High-order modes of spoof surface plasmon polaritons on periodically corrugated metal surfaces," Progress In Electromagnetics Research M **8**, 91-102 (2009).
27. M. Ordal, L. Long, R. Bell, S. Bell, R. Bell, R. Alexander Jr, and C. Ward, "Optical properties of the metals al, co, cu, au, fe, pb, ni, pd, pt, ag, ti, and w in the infrared and far infrared," Appl. Opt. **22**(7), 1099-1119 (1983).
28. K. Johansen, H. Arwin, I. Lundström, and B. Liedberg, "Imaging surface plasmon resonance sensor based on multiple wavelengths: Sensitivity considerations," Rev. Sci. Instrum. **71**(9), 3530-3538 (2000).
29. H. Hirori, M. Nagai, and K. Tanaka, "Destructive interference effect on surface plasmon resonance in terahertz attenuated total reflection," Opt. Express **13**(26), 10801-10814 (2005).
30. A. Otto, "The surface polariton response in attenuated total reflection," in Polaritons: Proceedings of the the First Taormina Research Conference on the Structure of Matter, E. Burstein and F. Demartina, ed. (Pentagon, New York, 1974), pp. 117-121.31. B. Reinhard, K. M. Schmitt, V. Wollrab, J. Neu, R. Beigang, and M. Rahm, "Metamaterial near-field sensor for deep-subwavelength thickness measurements and sensitive refractometry in the terahertz frequency range," Appl. Phys. Lett. **100**(22), 221101 (2012).
32. L. J. Sherry, S.-H. Chang, G. C. Schatz, R. P. Van Duyne, B. J. Wiley, and Y. Xia, "Localized surface plasmon resonance spectroscopy of single silver nanocubes," Nano Lett. **5**(10), 2034-2038 (2005).
33. B. Ng, S. Hanham, V. Giannini, Z. Chen, M. Tang, Y. Liew, N. Klein, M. Hong, and S. Maier, "Lattice resonances in antenna arrays for liquid sensing in the terahertz regime," Opt. Express **19**(15), 14653-14661 (2011).
34. C.-Y. Chen, I.-W. Un, N.-H. Tai, and T.-J. Yen, "Asymmetric coupling between subradiant and superradiant plasmonic resonances and its enhanced sensing performance," Opt. Express **17**(17), 15372-15380 (2009).

1. Introduction

There are two important technologies that are inspiring new technical developments for biosensing: plasmonics and terahertz. Surface plasmon polaritons (SPPs) are travelling charge density waves at the surface of conducting materials. Surface plasmon resonance (SPR) is the coupling resonance of SPPs at the interface of two media (metal-dielectric) with permittivities of an opposite sign [1-3]. The SPP oscillations are associated with a large enhanced electric field that decays exponentially in the perpendicular direction. As a result, a SPP is very sensitive to a change of the dielectric environment near the interface. The basis of the approach of SPR sensing is the change of the resonance condition with the change in the contacting medium. Although the first the observation of SPP was reported more than a century ago [4], the use of SPR as a sensing application began with the appearance of the practical coupling method, called attenuated total reflection (ATR) [5, 6], which enable the optical excitation of SPPs. The SPR

technique has been an important research tool in biophysics because it can measure the refractive index or optical absorption with high sensitivity [7]. SPR has also been widely used in the biology and biochemistry fields [8], particularly for label-free biosensing [9], and it can monitor the kinetics of biological processes in real time [10, 11].

During the last few years, another increasing focus has been placed on terahertz technology because terahertz radiation (λ = 30 μm - 3 mm) has unique advantages, for example, terahertz radiation has the ability to penetrate clothing. Terahertz technology is very useful for modern non-invasive security systems [12] and the next generation of high-speed broadband communication systems [13]. Another promising application of terahertz technology is biosensing. The interest in terahertz biosensing is due to the large number of molecules that have their collective vibrational and rotational modes in this frequency region [14, 15]. As a result, terahertz sensing is significant for numerous environmental, medical, and industrial sensing applications.

In principle, the combination of the high sensitivity of SPR and broadband "fingerprint" spectra of terahertz can be used for numerous applications of terahertz biosensing. However, beyond the use of the visible wavelength regime, the use of the terahertz spectral region of SPR sensing has rarely been investigated. This lack of terahertz SPR sensing is because the refractive index of most noble metals is extremely high in the terahertz regime and the intrinsic plasma frequencies of noble metals always resides in the ultraviolet frequency region. Consequently, SPPs in the terahertz regime on a smooth metal-dielectric interface, for example, a Zenneck wave [16], are weakly bound to the interface, and the penetration depth into dielectric is several centimetres. The penetration depth into the dielectric is a crucial parameter in SPR biosensing because a large penetration depth corresponds to a low intensity of the electromagnetic field around the interface. A weakly bounded field exhibits a weak interaction between the radiation and analyte, which limits the sensitivity of the terahertz SPR sensing.

The drastic difference between SPPs in the visible and mid-IR frequency domains has fuelled research into alternative means to confine propagating radiation to sub-wavelength scales at terahertz frequencies. Metamaterials modified with micro-structures possess a lower effective plasma frequency, which can also support a confined surface wave in the form of a spoof surface plasmon polariton (SSPP) [17-20]. The exploitation of THz spoof surface plasmon resonance opens up new developments in terahertz SPR sensing. Most terahertz SPR techniques are based on the Kretschmann configuration [5] and are often used in surface plasmon enhanced infrared reflection absorption spectroscopy [21], which can enable an molecular absorption enhancement of even hundreds time due to localised field enhancement on the textured metal surface [22]. In addition to spectroscopy, the SPR in the terahertz regime is also used for imaging [23]. The mid-IR biological sensing application based on prism-coupling to SPP modes are also investigated [24]. The basic theory of this type of SPR sensing is that the resonant wavelength or incident angle will shift with the change in the surface composition to satisfy the SPP resonance condition. Recently, the combination the benefits of the inherent macro-channels and plasmonics of an array-grooved corrugated spoof plasmon metal surface was demonstrated to have enormous potential for high sensitive terahertz SPR sensing for fluidic analyte [25].

In this paper, we further investigated the use of a high-order mode of spoof SPPs for terahertz SPR sensing based on the concept recently reported in the literature [25]. First, we introduced the configuration of a proposed terahertz SPR sensor and discussed the dispersion relation of a spoof SPP wave. Next, we analysed the influence of the gap distance between the prim base and the metal film surface on the resonance for different SSPP modes. Finally, terahertz SPR sensing with an optimal gap was examined by characterising analytes of different refractive indices, and a comparison of the sensitivity of the fundamental mode SSPP and the high-mode SSPP based sensing approaches was also performed.

2. Configuration of surface plasmon resonance sensing

The spoof SPP is excited using an Otto prism coupling configuration [6], as shown in Fig. 1, which can be easily implemented using a terahertz-time–domain spectrometer. A prism with refractive index n_p is used to increase the wavevector for phase matching. A thin metal film beneath a prism with *a* coupling gap, *h*, is used to support a spoof SPP. A dielectric medium with permittivity ε_d is filled into the gap and grooves. Unlike a traditional smooth film, the proposed metal film is penetrated by a linear array of subwavelength grooves with period *p*, width *w*, and height *h*. The advantages of such an integrated structure are that the groove can serve as the microfluidic channels that enable the terahertz sensing of liquid or gas, thereby significantly reducing the sample consumption and allowing for a more accurate real-time detection of the reaction occurring inside the microchannels due to reduced turbulence.

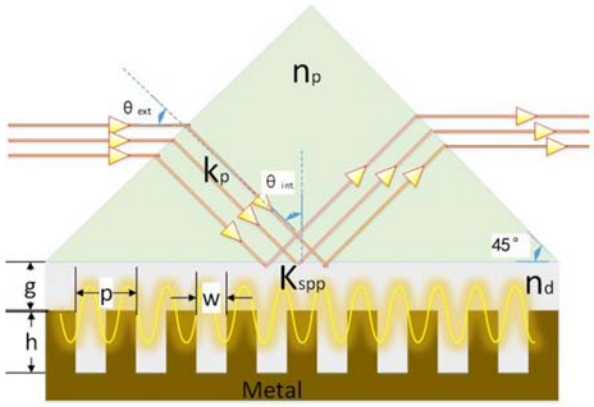

Fig. 1. Otto geometry of the surface plasmon excitation in the attenuated total reflection regime using a high-refractive-index prism and a periodically grooved metal film. Grooves are of width *w*, depth *h*, and periodicity *p*. *g* is the distance of the gap between the prism base and the surface of the metal film. $k_{0,}k_p$ are the wavevectors in free space and in the prism, respectively; k_{spp} is the wave vector of the surface plasmon wave. θ_{ext} is the external angle with respect to the normal line of the prism facet, and θ_{int} is the incident angle at the base of the prism. The resonance reflectivity approaches zero, and the off-resonance reflectivity approaches unity.

A collimated terahertz beam with angle θ_{ext} is injected through the left facet and refracted to the bottom face with an internal incident angle θ_{int}. After interacting with the analyte inside gap, the modulated radiation will reflect off the prism base and then exit the right facet of prism to be detected. The reflectivity will exhibit a sharp minimum at the frequency corresponding to the surface plasmon excitation. Thus, we can determine the dielectric parameters of the groove-filling medium by measuring the reflection spectrum. Note that to couple the incident radiation into the spoof plasmon wave, θ_{int} must be larger than the critical angle, $\theta_c = \arcsin n_{\text{air}} / n_{\text{p}}$, to form the evanescent wave that results from total internal reflection. θ_{int} can be calculated through following expression by applying Shell's law:

$$\theta_{\text{int}} = \arcsin\left(\text{n}_{air}\sin\theta_{ext}/\text{n}_{\text{p}}\right) + 45^{\circ} \qquad (1)$$

where n_{air} is the air refractive index, which is equal to one. The value of the angle of 45 degrees is the inner angle of the prism. The incident light beam in the prism has a wavevector $k_p^2 = k_{//}^2 + k_\perp^2$, where $k_p = n_p \omega / c$; $k_{//}$ and $k_\perp$ are the parallel and perpendicular components of the wavevector, respectively. The excitation of a SPR requires the parallel component of the electromagnetic field to satisfy the momentum matching condition:

$$k_{spp} = k_{//} = \frac{2\pi}{\lambda_0} n_p \sin(\theta_{\text{int}}) \tag{2}$$

3. Dispersion relation of the spoof SPP

k_{spp} is the wavevector of the SSP wave on the periodic grooved surface. In the limit of $w, p << \lambda$, the collective response of the array of grooves can be approximated using effective medium theory, which yields the plasma-like response with an effective plasma frequency [17]. Taking the metal loss into consideration, the dispersion relation of a spoof plasmon wave on a grooved corrugated metal surface can be expressed as [20]:

$$k_{spp} = \left(\varepsilon_d k_0^2 + \left(\frac{w}{p} \right)^2 k_d^2 \tan^2 (k_d h) \right)^{1/2} \tag{3}$$

where

$$k_d = k_0 \sqrt{\varepsilon_d} \left(1 + {}^{l_s(i+1)}\!/_{w} \right)^{1/2} \tag{4}$$

ε_d is the permittivity of the medium filling in the grooves and the semi-infinite space; ε_m is the complex permittivity of metal film; w, p, h are width, period and depth of groove; $k_0 = 2\pi f / c$ is the vacuum wavevector; and $l_s = \left(k_0 \operatorname{Re} \sqrt{-\varepsilon_m} \right)^{-1}$ is the skin depth of the metal. From Eq. (4), we can see that the dispersion relation is determined by the subwavelength structures. That is, the spoof SPP structures have significant design flexibility because the effective plasma frequency can be designed across the desired range of frequencies, which is very important for biosensing. In fact, the dispersion is primarily dependent on the groove depth h [17, 19]. When h is large enough, i.e., $h > mp$ (integer m is the order of the mode, p is the period of array-groove), the high mode of spoof SPP with the order of m begin to be supported; while for the case of $h < p$, there is only the fundamental mode spoof SPP wave on the corrugated metal surface [26]. To understand the origins of the higher modes, we can view the metal grooves as the 1D cavity with a narrow slide opening to air, then we can realize the electric field inside groove possesses a series of resonant frequencies, at which $k_0 h = m\pi$, where m are positive integers, i.e. the mode orders of resonances. When the gap depth h is larger than $m\pi / k_0$, the corresponding mth-order resonance is supported. Because of the opening of the groove end, a small amount of electromagnetic field will extend into air and the "extending" electric field from adjacent grooves couple with each other and finally form the propagating wave. In fact, in the first Brillioun zone, the wavenumber of propagating wave on corrugated surface, k_0, is limited within π/p, i.e., $k_0 < \pi / p$; thus, the condition of existence of mth-order resonance in grooves, $h > m\pi / k_0$, is consistent with criteria of appearance of mth-order spoof SPP wave, $h > mp$. Therefore, each propagating mode of SSPP can be considered the transfer of a corresponding modified resonant mode along the surface through coupling between the opening cavities. The more details about the high mode of SSPP can be found in the great work Ref. 26. We used the finite-element method (FEM) to calculate the dispersion of a periodically

grooved metal film with the geometry of h =100 μm, p = 60 μm, w = 20 μm (using the eigenmode solver of *COMSOL multiphysics*). In the calculation, the metal film was supposed to be Au, as described by the Drude mode, with a plasma frequency $\omega_p = 1.367 \times 10^{16}$ Hz and a scattering frequency $\gamma = 4.072 \times 10^{13}$ Hz [27].

The dispersion relation curves obtained from Eq. (3) and the FEM calculation are shown in Fig. 2. The small departure between the analytical line and the numerical line in the high mode regime is due to the lack of consideration of high mode diffraction in Eq. (3). The insets are the electric field distribution for the fundamental mode SSPP and the high mode SSPP at $k_{spp} = \pi / \mathrm{p}$. The appearance of one node inside groove shown in the right inset prove that it is the SSPP with mode order m=1, which is consistent with the mentioned criteria of existence of high modes. In addition, the high mode SSPP exhibits more confinement of the electric field than fundamental mode. For both of the modes, the dispersion plots become flat and the wavevector becomes infinite as the frequency approaches the edge of first Brillioun zone. The dashed dot line is the dispersion relation for vacuum light, and the dashed straight line is the dispersion relation for parallel wavevector $k_{//}$ in the prism. With a proper θ_{int}, the $k_{//}$ line crosses the SSPP dispersion curves, forming two intersections, indicated as dots A and B. The intersection point determines the expected resonance frequency f_{res} at which the incident THz radiation will couple into the spoof surface plasmon wave.

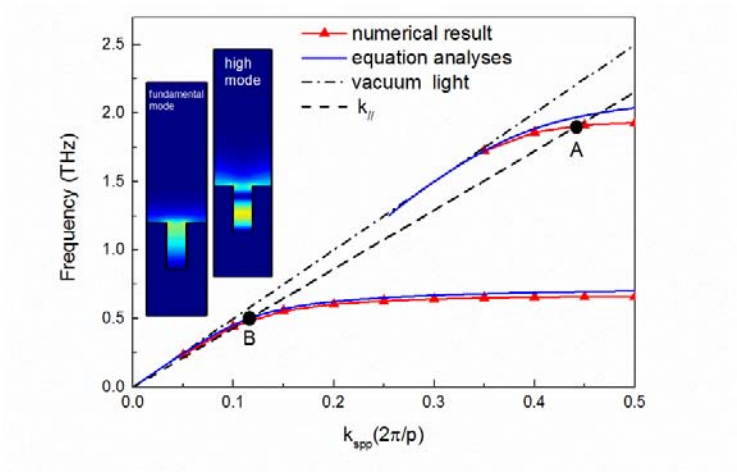

Fig. 2. Dispersion relation of the SSPP of periodic grooves with p = 60 μm, w = 20 μm, and h = 100 μm. The blue solid lines are calculated from Eq. 3, and the red lines with triangle symbols are obtained using *COMSOL* software. Obviously, there are two branches that correspond to the fundamental and high modes of SSPP. The dashed dot line is the dispersion relation of the light in vacuum, and the dashed straight line is the dispersion relation of the parallel wavevector $k_{//}$ of horizontal incidence. Theoretically resonance will occur at the intersections A and B. The insets show the electric field distributions for different modes of SSPP at the edge of first Brillouin zone, $k_{spp} = \pi / p$ (left for the fundamental mode, and right for the high mode). The dielectric function of the surrounding medium is set be one in the calculation.

4. Optimal gap distance for efficient coupling of an evanescent wave to the SSPP

The range of frequencies where SPR is excited is determined by the dispersion relation curves of light and the spoof SPP. To determine the resonant frequency f_{res}, 2D simulations were performed to obtain the reflectivity values for various wavelengths at different gaps h (using *COMSOL Multiphysics*). The simulation model is the unit cell with a single groove, shown as most-right inset in Fig. 3. The periodic port was used to inject P-polarised radiation, and Floquet periodic boundary conditions were applied along the direction of periodicity. The material of metal film was set as Au and was modelled using the Drude model. In our simulation, the coupling prism consists of K9 glass, with a refractive index n_p = 1.5163. All of the geometrical parameters are the same as those mentioned previously, and the gaps h= 100 μm and 400 μm were chosen as the representation of small and large distances, respectively. The incident angle θ_{int} is set to 50 degrees that meet the condition of total reflection at n_d =1.0, , i.e., $\theta_{\text{int}} > \theta_c = 41.26^\circ$.

Figure 3 shows the reflection spectra for gaps h = 100 μm and 400 μm with a horizontal injection. Obviously, two dips in the reflectivity spectrum were generated, which corresponded to the resonances of the different modes of SSPP predicted by the existence of the two interactions shown in Fig. 2. The two resonant frequencies were approximately 0.49 THz and 1.91 THz, respectively. Although they are in very good agreement with the expected frequencies, i.e., 0.5 THz and 1.91 THz for the intersection points A and B, respectively, some deviations exist between them. These deviations occur because the propagating surface plasmon is not the theoretical surface wave when the gap is small; as a result, a considerable part of the energy will reradiate back into the prism [28]. The reradiation will affect the surface plasmon dispersion relation. In addition, the energy damping [6] and destructive interference effect [29] also affect the shift of resonance.

In addition to the appearance of a dip, we also observed that the gap distance g has an import influence on the shape of dip or coupling efficiency for different mode SSPPs. At a small gap, i.e., h = 100 μm, the resonance reflectivity of the high mode SSPP exhibits a shaper dip, whereas the resonance of the fundamental mode exhibits a broadening and a shallow dip. On the contrary, for the large gap of h = 400 μm, the resonance at the fundamental mode was strong, with a sharp dip in reflection, but the high mode surface plasmon resonance was not excited. This behaviour is expected because electric field extensions of different mode SSPP are different, i.e., the fundamental mode SSPP decays more slowly in the vertical direction than does the high mode SSPP. The penetration length of the evanescent wave under the prism is finite and certain. When the gap distance is too large, the evanescent wave cannot reach the region of the mode field of the high mode SSPP; therefore, the resonance of the high mode cannot be excited. In contrast, fundamental mode SSPP will achieve good coupling because it has more overlap of the electromagnetic field with the evanescent wave due to its large mode field distribution. Conversely, when the gap distance is small, the evanescent wave can be coupled into a high mode SSPP efficiently; however, the close proximity of the prism will significantly increase the scattering, resulting in poor coupling to the fundamental mode SSPP.

From the time-average energy density distribution of different mode SSPRs, shown as insets in Fig. 3, we also found more clear evidence of the effect of gap distance on the SSPPs. For the small gap distance of g = 100 μm, the high mode resonance, inset (b), has a stronger energy confinement than the fundamental mode, inset (a); the fundamental mode SPR at the large gap distance, inset (c), has more energy coupling to the SSPP than the small distance case, inset (a). The arrows linearly represent the magnitude and direction of time-average power flow of propagating spoof SPP wave. The considerable power flowing in the prism in the cases of small gap distance, indicated by the arrows in insets (a), confirm the reradiation into the prism of the fundamental mode SPP. The leakage of energy into the prism is mainly due to the reflection resulting from incomplete coupling to spoof SPP wave and the propagating SSPP

wave reradiation caused by the scattering at the edges of grooves. In fact, the involvement of the prism makes the coupling mechanism complicated, especially when the gap distance is small. In summary, the coupling strength of different mode SPPs can be finely tuned by the appropriate choice of the gap distance.

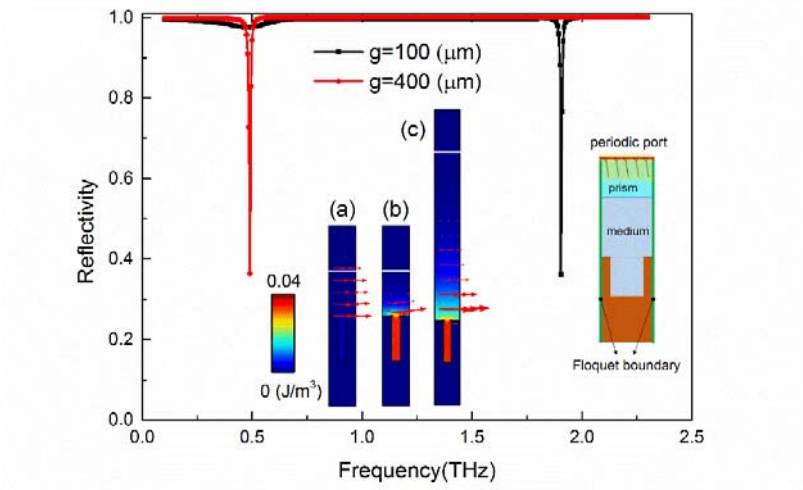

Fig. 3. Reflectivity at gaps of g = 100 μm and 400 μm. Two dips ($f_{\mathrm{res1}} \approx 0.49\mathrm{THz}, f_{\mathrm{res2}} \approx 1.91\mathrm{THz}$) are observed in the reflection spectrum, which correspond to surface plasmon resonance of the fundamental and high modes. Insets (a) and (b) are the time-average energy density distribution at f_{res1} f_{res2} , respectively, for g = 100 μm, and inset (c) is average energy density distribution at f_{res1} for g = 400 μm. The most right inset is the simulation model, showing a unit cell of the periodic groove. The metal film is set as Au, as described by the Drude model.

To achieve the optimal g for each mode SPR at which the reflectivity achieves a minimum value, we plotted the reflection spectra for various g values with different filling media, as shown in Fig. 4. The reflectance of the resonance was observed to initially decrease as the gap increased, reach a minimum, and then increase. This response indicates that the gap has an optimal value for the highest coupling efficiency. As can be seen from Fig. 4, except for the change of the peak value, a frequency-shift in the SPP resonance was observed with decreasing the gap distance. The frequency-shift originate from the interference effect between the electromagnetic wave reflected at the prism-air interface and that reemitted from excited surface plasmons, which depend on the wave vector of evanescent wave, the refractive index of prism, the incident angle of terahertz pulses and the distance between the prism and active material [29]. The frequency shift had also been explained using the additional damping mechanism, which comes from the presence of the prism [6]. The absolute ratio of the frequency shift Δf to the intrinsic resonance f_{spp}, $|\Delta f / f_{spp}|$, is in the order of 0.001[30]. Another notable phenomenon shown in Fig. 4 is that the dip-frequency does not shift, but the peak of the reflectivity decrease with the increasing g when g is larger than the optimal gap g_{opt}. This result indicates that the surface plasmon resonance at a sufficiently large gap distance is the instinct SSPP on a corrugated film, without the impact of prism's approaching. The results in Fig. 4 verify that the frequency-shift is indeed very small and thus the impact of the frequency-shift can be neglected in identifying the resonance location.

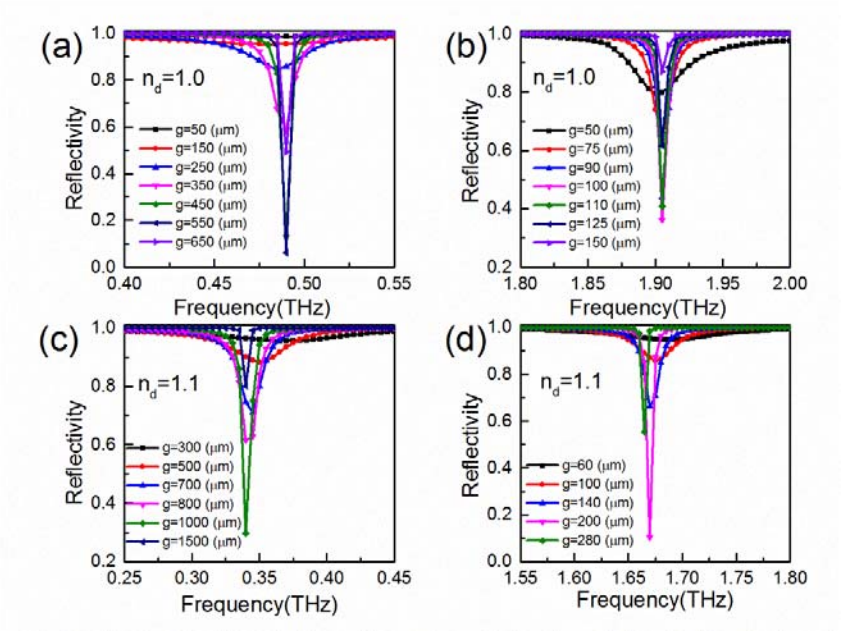

Fig. 4. Simulated reflectivity spectra of different mode SPRs for different gap distances: (a) for the fundamental mode SPR at $n_d = 1.0$; (b) for the high-order mode SPR at $n_d = 1.0$; (c) and (d) are for fundamental mode and high mode SPR of $n_d = 1.1$. The dips correspond to surface plasmon resonances. The deeper the dip, the more efficient the evanescent wave coupling into the spoof SPP.

The fact that the dip could be tuned by changing the gap distance reminded us that the detection sensitivity of the SPR measurement could be improved if the gap distance is optimised to the point at which the dip-peak value is minimised. We fitted the peak values versus the gap distance and approximately obtained the optimal gaps $g_{opt}{}^{1} = 509um, g_{opt}{}^{2} = 100um$ for the fundamental and the high modes of SPR sensing for n_d=1.0 , and the optimal gap for fundamental and high modes for n_d=1.1 are about 1000 μm and 200 μm, respectively. It was seen that the optimal gap for n_d=1.1 is larger than that for n_d=1.0 . In fact, the optimal gap is determined by the compositive effect from extension of evanescent wave on prism base and the confinement of SSPP wave. The extension of evanescent wave, defined as the decaying length to 1/e, is expressed as: $L_1 = \lambda / (2\pi\sqrt{(n_p \sin(\theta_{\text{int}})^2 - n_d{}^2)})$,the confinement of SSPP wave, defined as the decaying length to 1/e, is expressed as: $L_2 = \lambda / (2\pi\sqrt{((k_{spp} / n_d k_0)^2 - n_d{}^2)})$,where $k_0 = 2\pi f / c$ is the vacuum wavenumber, k_{spp} is the wavevector of SSPP wave obtained by Eq. 3. Calculated by using these two equations L1+L2 increases with the increasing of n_d. This increase will lead to a small amount of the "extended" electromagnetic field reaching the groove edges, which give rise to a reflection and a resulting reduced coupling efficiency comparing with the optimized coupling regime. In other words, the preset optimal gap is insufficient to support an optimal coupling for increased n_d. Generally, the corresponding optimal gap increase with the increase of n_d.

5. Samples with different refractive indices characterized by different mode spoof SPRs

We examined the performance of the different mode spoof SPR-based sensing via simulation-testing of a dielectric medium with various refractive indices n_d. Because an evanescent wave only appears when the refraction index of the filled medium (n_d) is smaller than that of the prism (n_p) and the SSPP coupling occurs when $n_p \sin(\theta_{\text{int}})$ is equal to k_{spp}/k_0 that is larger than n_d, we considered few samples with the refractive indices of n_d = 1.0, 1.05, 1.1, and 1.15 to test our sensing system. Note that the maximum detectable refractive index is limited within $n_p \sin(\theta_{\text{int}})$, therefore the measurement of samples with larger refractive indices can be expected if a larger incident angle or a larger refractive index prism are employed.For each sample, we performed simulations at the optimal gap distances, i.e., $g_{opt}{}^1$ and $g_{opt}{}^2$.

The comparison of the reflectivity for different mode sensing is shown in Fig. 5(a). The results clearly demonstrated that for both the fundamental mode and the high mode SSPP sensing, the resonance exhibited a red shift as the refractive index n_d increased. Besides, the displacement of the adjacent resonances of high mode sensing was larger than the corresponding displacement of fundamental mode sensing. This result indicated that the high-mode SSPP-based SPR sensing has a higher sensitivity than the fundamental mode. However, as the refractive index deviates from the optimal value, i.e., $n_2 = 1.0$, the resonant dip becomes broadened and its value increases. This behaviour can be attributed to the fact that the change of n_d affects both the dispersion relation of the spoof SPP and the penetration depth into the medium of the evanescent wave on the base of prism. Thus, the further n_d departed from the predesigned value at the optimised coupling configuration, the more thoroughly the optimal coupling regime became broken.

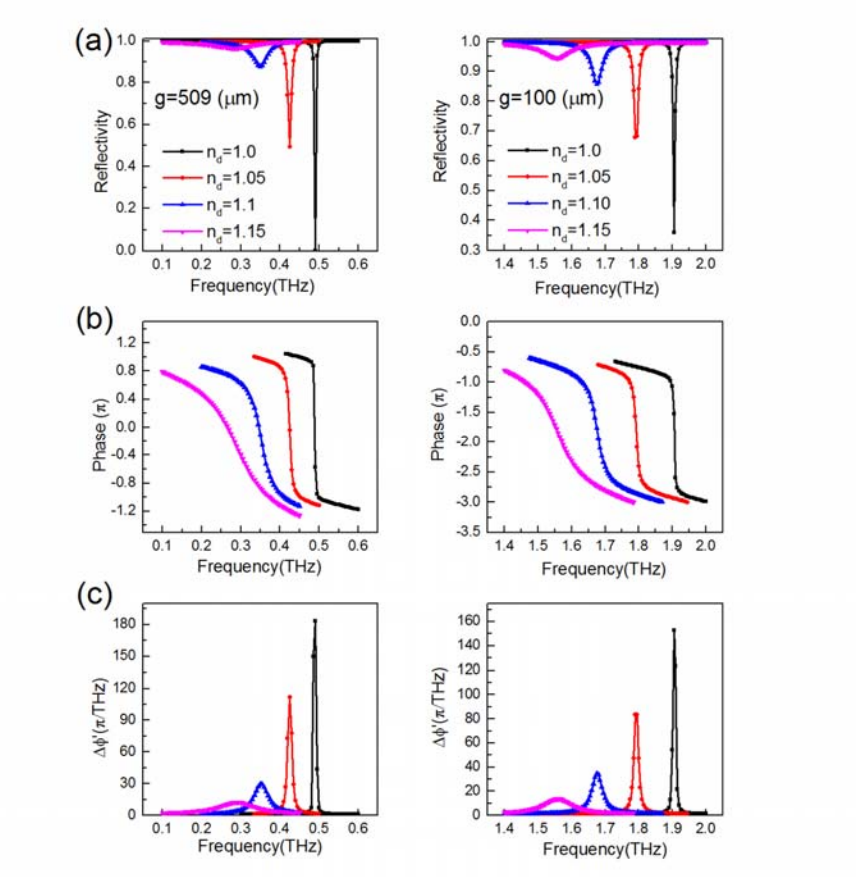

Fig. 5. Reflectivity and phase change spectra for different dielectric media with various refractive indices n_d for different mode SSPP sensing at the optimal gap. (a) Reflectivity for different n_d; (b) phase change $\Delta\varphi$; (c) absolute gradient of $\Delta\varphi$, $\Delta\varphi'=\left|d(\Delta\varphi)/df\right|$. The left part is for the fundamental mode SSPR sensing, and the right part is for high mode SSPR sensing. Note the phase in (b) are extended to show a monotonous change.

The broadening of the dips hinders the accurate identification of the resonance frequency from the reflectivity spectrum. Fortunately, except for the minimum amplitude of the reflection spectrum, another tell-tale sign of surface plasmon resonance is the sharp phase jump at the resonance frequency [25]. The phase change ($\Delta\varphi$) is the difference in phase of each frequency component between the sample and reference. The reference signal is measured in the absence of the prism, which can be mimicked by substituting metal with perfectly matching layers (PML). As shown in Fig. 5(b), the phase change exhibits a step jump near the resonance frequency. Note that the phase region was extended to show a monotonous change. A further clear identification of resonance could be achieved through the absolute gradient of the phase change, $\Delta\varphi' = |\, d(\Delta\varphi)/df\,|$, as shown in Fig. 5(c). The $\Delta\varphi'$ spectrum was found to exhibit a sharp peak at the resonance frequency, corresponding to the sharp phase change. It is remarkable that even for the case of $n_d = 1.15$ close to the detection limit, $n_p \sin(\theta_{\text{int}}) = 1.16$, where the reflection dip is relatively boarded and shallow, the peak in $\Delta\varphi'$ spectrum is still discriminative.

6. Comparison of the sensing sensitivity of fundamental and high modes of SSPPs

To present a direct comparison of the sensitivity of the fundamental and the high modes of SSPPs, we plotted the resonance frequencies against the refractive indices for the two modes of SSPR sensing in Fig. 6. We found that for either the fundamental mode or the high mode of SSPP-based sensing, the relationship between the resonance frequency and the refractive index remained highly linear. The dashed and solid lines shown in Fig. 6 are the linear fittings given by $f_{sp1} = 1.76 - 1.28 n_d$ and $f_{sp2} = 4.17 - 2.27 n_d$ which offer the sensitivities of 1.28 THz RIU^{-1} and 2.27 THz RIU^{-1} for the fundamental mode and high mode based sensing, respectively. Obviously, the sensitivity featured by high mode SSPP is higher than that of the fundamental mode SSPP. It is noted that the result in fact will be affected by the experimental limitation such as frequency resolution which will determine the minimum detectable change in refractive index n_d. For our setup, a detection limit of 0.004 RIU can be obtained for the high mode based sensing assuming a detection frequency-resolution of 10GHz. The sensitivities are better than that reported in similar devices [25, 31]. Thus, the higher sensitivity makes the high mode SSPP-based sensing approach very promising for sensing small change of the refractive index.

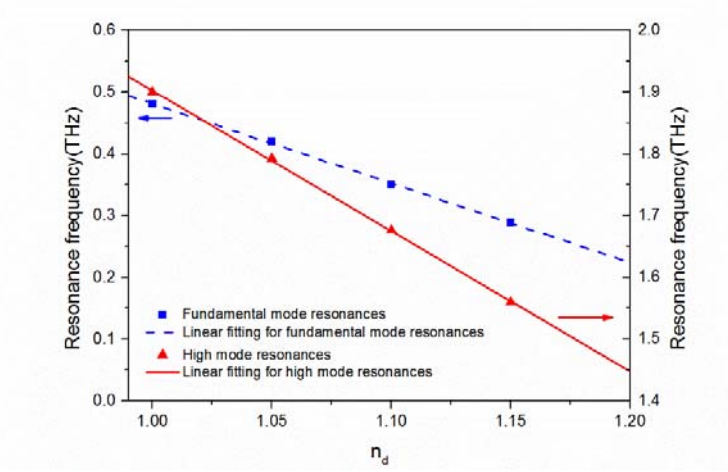

Fig. 6. Resonance frequencies versus refractive indices. The dashed and solid lines are the linear regression fits of the resonance frequency corresponding to a sensitivity of 1.28THz/RIU and 2.27THz/RIU for the fundamental mode and the high mode SSPP-based sensing, respectively.

If we used $\Delta\phi'$ as our sensor readout response, the figure of merit defined as FOM= $(df_{sp}/dn)/\Delta f_{sp}$ can be used to estimate the performance of SSPP-based sensing [32]. df_{sp}/dn is the change in resonance frequency per refractive index change, and Δf_{sp} is the FWHM of resonance in the $\Delta\varphi'$ spectrum. The FOM values of high mode SSPR sensing for n_d = 1.0, 1.05, 1.1, and 1.15 were 262, 157, 46, and 216, respectively. The values were larger than the values of fundamental mode SSPR sensing (148, 89, 26, and 12). The FOM decreased with the increasing n_d because the further n_d departed from the predesigned value for the optimised coupling configuration, the more thoroughly the optimal coupling regime became broken that results in a broader and shallower dip of SPR and therefore a larger FWHM. Hence, the FOM value, which is inversely proportional to FWHM, decreases with increasing n_d.These FOM values for the fundamental and high modes are much higher than the results reported

previously [33, 34]. It is worth mentioning that our simulated FOM is far larger than the experimental result from a similar setup with shallow groove, for example, FOM=49 for nitrogen (n_d =1.0) [25]. To the best of our knowledge, the obtained FOM results represent the highest values of terahertz sensing ever reported. Note that such a high resolution can only be achieved for a weakly absorbing sample. In general, the FOM of sensing decreases with the increasing loss in the sample material. Overall, the high mode SSPP-based SPR sensing is superior to that of the fundamental mode. The improvement of the sensitivity and the high FOM for the high mode SSPP sensing is attributed to its strong confinement of the electric field. This enhanced electric field, resulting from high confinement of the high mode SSPP, could be a very interesting advantage if used to detect a small amount of analyte because it offers a strong interaction.

7. Conclusions

In summary, we investigated the performance of different modes of terahertz SSPP-based sensing of refractive index changes. Metal film corrugated with a periodic array of subwavelength grooves was used to support a fundamental mode SSPP and a high mode SSPP, and an Otto-prism setup was used for excitation of the surface plasmon resonance. The coupling efficiency of the evanescent wave to the SSPP was found to depend on the gap distance between the prism base and metal film surface. For a given filled medium with a certain refractive index, there was a corresponding optimal gap distance at which the strongest coupling occurred. The result of testing filled dielectric media with different refractive indices demonstrated that high mode SSPP-based sensing had an improved sensitivity of 2.27THz RIU^{-1}, which nearly doubled the sensitivity of the fundamental mode. The results highlighted the fact that the feasibility to "tune" the resonance to the most efficient coupling state by modulating gap distance allows for high sensitivity detection of a specific analyte. Furthermore, the tuneable spoof SPP could be used to conduct sensing over a wide frequency range because the response of the spoof SPP can be easily engineered by redesigning its geometrical parameters. The inherent macro groove channels of the proposed sensing platform not only facilitate enhanced transport of reactants to the active surface but also improve the sensitivity by utilising its support of high mode SSPPs, making it a promising approach for a sensor for numerous analytes, including gaseous and fluidic molecules.

Acknowledgements

We gratefully acknowledge support from the National Natural Science Foundation of China (51005077), the Fujian Provincial Excellent Young Scientist Fund, the Training Program of Fujian Excellent Talents in Universities, the Specialised Research Fund for the Doctoral Program of Higher Education, the Ministry of Education, P.R. China (20133514110008) and the Ministry of Health, P.R. China (WKJ-FJ-27).